Ultrahigh-Speed Color Imaging with Single-Pixel Detectors at Low Light Level

Weigang Zhao,[1] Hui Chen,[1,*] Yuan Yuan,[1,†] Huaibin Zheng,[1] Jianbin Liu,[1] Zhuo Xu,[1] and Yu Zhou[2]

[1] *Electronic Materials Research Laboratory, Key Laboratory of the Ministry of Education and International Center for Dielectric Research, Xi'an Jiaotong University, 28 West Xianning Road, Xi'an, China*

[2] *MOE Key Laboratory for Nonequilibrium Synthesis and Modulation of Condensed Matter, Department of Applied Physics, Xi'an Jiaotong University, 28 West Xianning Road, Xi'an, China*

(Received 2 May 2019; revised manuscript received 19 July 2019; published 25 September 2019)

Single-pixel imaging is suitable for low light-level scenarios because a bucket detector is used to maximally collect the light from an object. However, one of the challenges is its slow imaging speed, mainly due to the slow light-modulation technique. We here demonstrate 1.4-MHz video imaging based on computational ghost imaging with a red-green-blue light-emitting diode array having a full-range frame rate up to 100 MHz. With this method, the motion of a high-speed propeller is observed. Moreover, by use of single-photon detectors to increase the detection efficiency, this method is developed for ultrahigh-speed imaging under a low light level.

DOI: 10.1103/PhysRevApplied.12.034049

I. INTRODUCTION

Ultrahigh-speed imaging under a low light level is an indispensable diagnostic tool for many disciplines and applications, such as detecting biodynamics in living cells or observing microfluidic behavior [1–3]. It requires an imager having the capabilities of fast storage and processing of a large data flow. Simultaneously, that imager should be sensitive enough to detect a dynamic event within an ultrashort time. Nevertheless, to meet both of these requirements is challenging. For repetitive dynamic events, the second requirement can be worked around by repeatedly measuring the same event in an ultrashort time until the accumulated light energy is adequate to reconstruct a frame. Various high-speed imaging techniques for repetitive dynamic events have been developed in recent years, such as the pump-probe technique, use of a framing streak camera, and tracing the flight of a laser beam [4–13]. However, these techniques are unable to capture unique or random events (such as molecular motion in biological samples), limiting their uses in practical applications.

To image a nonrepetitive ultrafast event, a method must have the capability of continually recording images at a high frame rate and high sensitivity to capture enough light in a short time. Conventional spatially resolving detectors such as charge-coupled devices (CCDs) and complementary-metal-oxide-semiconductor devices are not suitable for ultrahigh-speed imaging under a low light level [14]. This is due to the compromise between the response speed of pixelated sensors and their sensitivity. Although a CCD imager with a frame rate of 1 MHz has been developed, it requires high-power illumination to acquire enough light for each pixel in the short time of a frame [15]. This bright illumination may damage samples in some scenarios, such as biological imaging.

Single-pixel imaging is an alternative way to realize ultrahigh-speed imaging [1–3,16–19]. It uses a temporal measurement approach to replace the spatially resolving detection scheme, and then uses an ultrafast and sensitive single detector to detect the light variance that was modulated by an object. One of the high-speed single-pixel-imaging methods is the photonic-time-stretch (PTS) technique, also named "dispersive Fourier transform and frequency-to-time mapping." The PTS technique stretches the broadband optical spectrum of an ultrashort laser pulse, and maps it into a two-dimensional (2D) spatial waveform that is projected onto the object. The field reflected from the object is recombined as (transformed into) a temporal waveform that is able to be measured with a high-speed single-pixel detector [2,3]. This technique has several drawbacks: (i) in each frame, the 2D spatial reflected light intensities are encoded into a temporal waveform, and the single-pixel detector is used to decode the spatial signals, which does not essentially increase the detection sensitivity; (ii) it is expensive due to the expensive ultrashort pulsed laser and the optical amplifier; (iii) it works only at certain optical wavelengths, which limits its applications, such as in color imaging or in imaging of some materials that have a bad response at the probing wavelengths.

*chenhui@xjtu.edu.cn
†yuanyuan0@xjtu.edu.cn

Ghost array as a light source to increase the imaging speed [29]. Similar research was independently announced in 2018 [30]. Here we develop a method to overcome the compromise between sensitivity and a high frame rate, and enable ultrahigh-speed imaging under a low light level. As a proof of this proposal, we demonstrate the following experiments: (i) imaging at a frame rate of 1.4 MHz for a fast rotating propeller sweeping a letter; (ii) high-speed imaging of a colored object; (iii) high-speed imaging under a low light level with single-photon detectors (SPDs) to increase the detection sensitivity, where the illumination on the object is less than 3×10^9 photons/s mm^2.

II. EXPERIMENT

The experimental setup is shown in Fig. 1. The light source is a self-made 10×10 LED array. Each element consists of a red, a green and a blue LED light bulb. A field-programmable-gate-array circuit is designed to simultaneously control all the LED bulbs to be *on* or *off* with a full frame rate up to 100 MHz. A sequence of arbitrary patterns can be loaded into the memory of the circuit from a computer via a USB port. Afterward, the stored patterns are emitted with a time interval of 10 ns (100 MHz), and are projected onto an object via a lens (lens 1 in Fig. 1). In experiments, we use Hadamard patterns. Since the order of a Hadamard matrix must be 1, 2, or a multiple of 4, the best base fitted to the LED array is of 8×8.

In the first experiment, a full set of 8×8 Hadamard patterns is prestored in the circuit. Immediately before the Hadamard patterns, we place a mark that consists of three sets of full white and full black patterns, which helps to precisely determine the start time of sending the patterns. All the patterns ($64 + 6 = 70$ in total, where "6" represents the flag patterns) are successively displayed. After the display cycle ends, another cycle keeps repeating until the end of the experiment. The light distribution on the object plane can be formulated as

$$M(x,y;t) = \sum_j P_j(x,y)\, W_\tau(t - T_{m,j}). \qquad (1)$$

Here $P_j(x,y)$ is the jth projected pattern. $W_\tau(t - T_{m,j})$ is a window function: it is 1 over an interval of $[T_{m,j}, T_{m,j} + \tau]$ (where τ is the time for which a pattern lasts), but 0 outside this region. $T_{m,j} = m \times T_c + j \times T_j$, is the starting time of the jth pattern in the mth cycle, where T_c is the total time of a cycle and T_j is the time between two adjacent patterns.

The object is a hollow letter T, immediately in front of which a propeller is rotating at 40 000 revolutions/min. The length of the propeller is about 5 cm. Thus, the linear speed at the edge is about 200 m/s. The light transmitted through the object is collected by a bucket detector (a photomultiplier tube with a bandwidth of 250 MHz). The bucket detector senses the intensity variance, which represents how the projected patterns were modulated by the object:

$$B(t) = \iint_s M(x,y;t)O(x,y;t)dxdy. \qquad (2)$$

Here $O(x,y;t)$ is the intensity-attenuation function of the object and $M(x,y;t)$ is the light-distribution function from Eq. (2). The integral indicates all the transmitted light from the object collected by the bucket detector. The second-order correlation is calculated as

$$G(x,y;t = mT_c) = \int_t^{t+T_\tau} M(x,y;t')B(t')dt', \qquad (3)$$

where $B(t')$ is the collected intensity as expressed in Eq. (3). $G(x,y;t = mT_c)$ represents the image of a dynamic object at time $t = mT_c$, which means that we reconstruct an image frame in every cycle. With the help of a mark, we are able to locate the time of the first pattern from the bucket signal, which is used to synchronize the times of the bucket signal and the projected patterns.

The motion of the propeller swapping T is captured with frame rates of 0.014 and 1.4 MHz (modulation rates of 1 and 100 MHz), as shown in Figs. 2(a) and 2(b), respectively. Please see the corresponding videos ac1MHz.avi and ac100MHz.avi. As shown in Fig. 2(a) frame by frame, the imaging speed of 0.014 MHz is not fast enough to capture all the motion of the propeller. Therefore, the frame rate of 1.4 MHz is necessary for such fast motion.

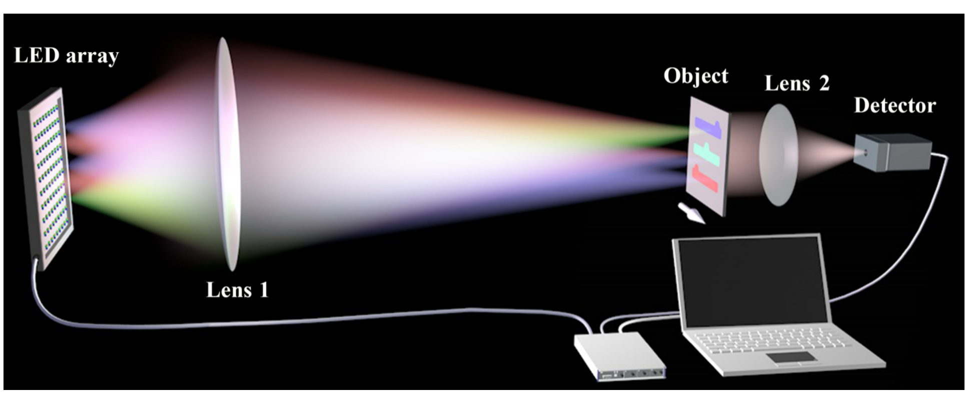

FIG. 1. The experimental setup for moving detection. The object consists of a static mask and a propeller rotating at 40 000 revolutions/min. Lens 1 is used to project the illumination patterns onto the object. The transmitted light from the object is collected by a photomultiplier-tube detector via a focusing lens (lens 2).

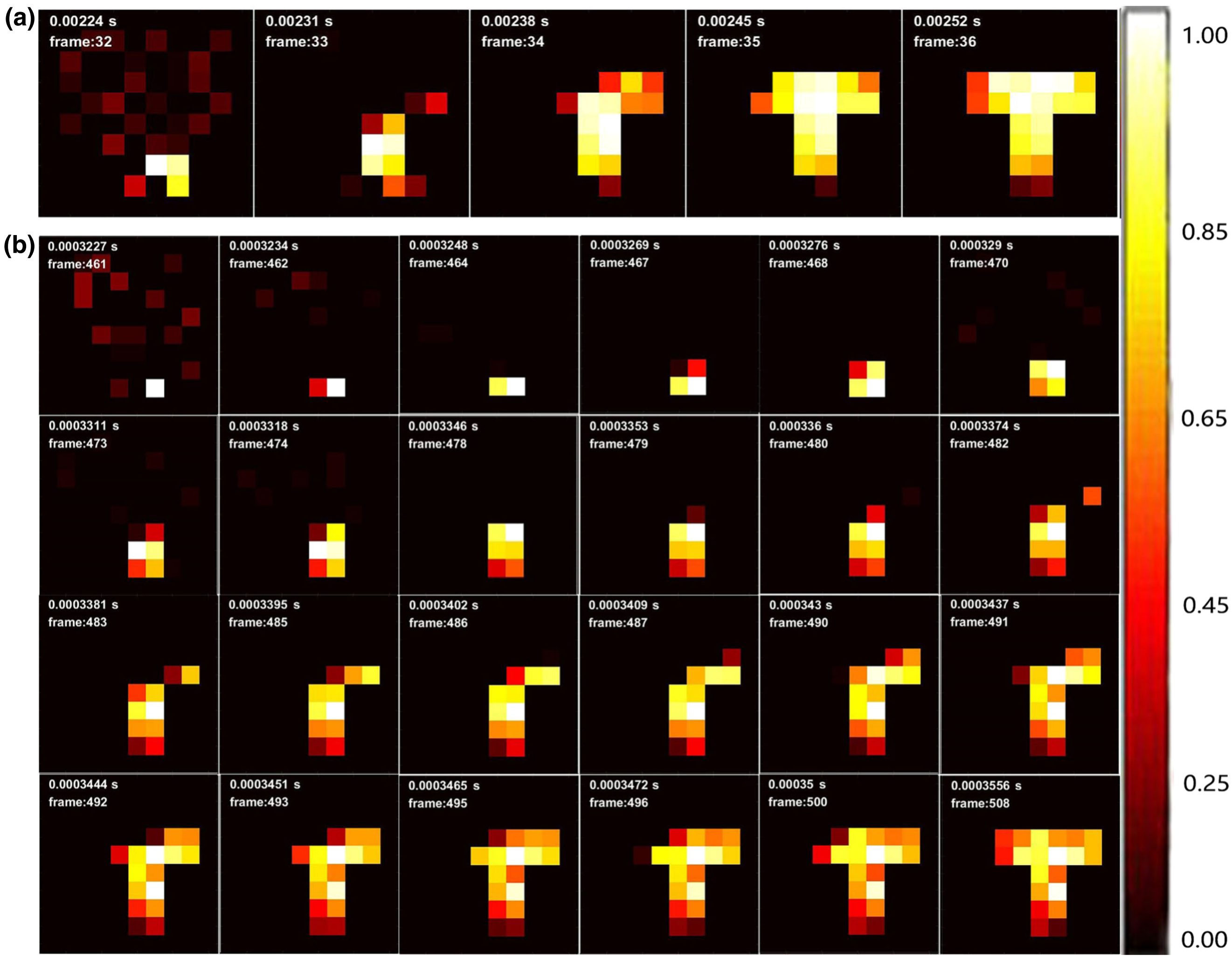

FIG. 2. The video frames of the imaging results: (a) imaging video with a 1-MHz speckle modulation rate; (b) video with 100 MHz modulation rate. Note that the images are enhanced with a background-removal process.

To perform color imaging, each Hadamard pattern is projected three times in red, green and blue, respectively. Therefore, the total number of subpatterns in a cycle is $6 + 64 \times 3 = 198$. The object consists of three plates in the three colors, as shown in Fig. 3. The object is placed on a moving stage moving from left to right at a speed of 20 mm/s. The blue illumination of our source is weaker than the green illumination and the red illumination, and the detector is also less sensitive for blue light. To achieve better imaging quality, the LED array is set to work at a frame rate of 1 MHz. The imaging frame rate becomes 5 kHz. Selected video frames are shown Fig. 4. See Ref. [41].

Under a low light level, the light intensity in a short integral time window is very weak. To increase the detection sensitivity, we instead use SPDs. A SPD will generate an electronic pulse as a count when photons arrive at the detector. Nevertheless, there are two drawbacks: (i) a count can indicate only the arrival of photons but cannot indicate the number of photons; (ii) after generating a count, it stops working for a certain time (so-called dead time). The dead time of our SPD is 80 ns, which means the maximum count in 1 μs (at a modulation rate of 1 MHz) is 12. This low dynamic range is insufficient to represent the variance of the intensity. A viable solution is to use multiple SPDs, which expands the dynamic range in proportion to the number of SPDs. Additionally, if the light-receiving system has a large field of view, it is hard to focus most of the light onto the small active area of a single SPD, and this also limits the range of the spatial modes that can be detected by the SPD, resulting in some components being missing in a recovered image. This problem can be effectively eliminated by use of multiple SPDs.

On the basis of the above analysis, we build an eight-SPD detection system and experimentally investigate the high-speed imaging under a low light level by photon counting. As shown in Fig. 5, eight multimode fibers (50 μm in core diameter) are close-packed at one end. At the other end, each fiber is connected to a SPD. The output

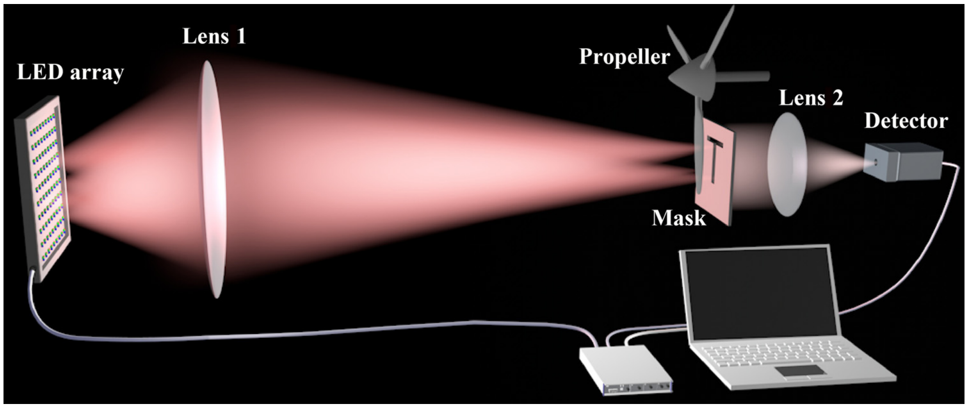

FIG. 3. The experimental setup for a colorful object. The object consists of three striplike objects in red, green, and blue, respectively. Lens 1 is used to project the illumination patterns onto the object. The transmitted light from the object is collected by a photomultiplier-tube detector via a focusing lens (lens 2).

signals from the detectors are fed into a time-correlated-single-photon-counting device that records the arrival time of each signal, from which we can know the number of photons in each time window.

We attenuate the illumination light to a level such that the light intensity falling on the detection plane is 3×10^9 photons/s mm^2. The focal length of lens 1 is 25 mm, which results in a spot of 2-mm diameter on the detection plane. To receive as many spatial modes as we can, a diffuser is placed 10 mm from the fiber tips, which scatters the light and mixes the spatial modes before they are incident on the fibers. On the other hand, the diffuser decreases the coupling efficiency by a factor of 10. Because of the 50-μm core diameter, the fill factor of the fiber receiver in an area of 4 mm^2 is approximately 6×10^{-4}. Thus, the total coupling efficiency is less than 6×10^{-5}. At the modulation rate of 1 MHz, the average photon number in 1 μs is less than 50. To achieve a better statistical result, we use ten cycles to recover a frame (i.e., the time of an imaging frame is 700 μs). A recovered imaging frame of a letter T is shown in Fig. 6.

The imaging speed is limited by the average photon number per modulation frame, which is influenced both by the coupling efficiency and the dynamic range. The dynamic range is defined as the maximum number of readout photons in the modulation time window, which is determined by the number of SPDs and their dead times. In our eight-SPD system, the dynamic range in 1 μs is 100, which is insufficient to recover a good image. However, this limitation can be easily overcome by modern detection technology. Commercial SPD arrays (32×32 [31], 256×256 [32]) have been announced and used in many fields, and can provide a dynamic range of more than 40 000. Meanwhile, a large number of pixels can effectively shorten the dead time of the whole detection system. Moreover, the large size of a SPD array will dramatically increase the coupling efficiency. With such SPDs, the imaging speed could be increased to 1 MHz or higher.

Currently, the array of our illumination device is only a 10×10 array, limiting its applications. Nevertheless, the resolution can be increased without changing the hardware configuration in some situations. Usually, the motion speed of a real object is quite slow in comparison with the modulation rate. A high-resolution image can be obtained by scanning an object with illumination patterns. In the experiment, an object of characters XJ is mounted on a 2D motorized stage, and then the object is scanned by the illuminating pattern horizontally and vertically, recording the coordination at the same time. In each scan, 1/18 of the object is imaged in 7 μs (with a modulation rate of 10 MHz). After scanning, an image with high resolution of 24×48 is retrieved, taking 126 μs in total. Figure 7 shows the reconstructed image of the whole object.

III. DISCUSSION

The imaging frame rate is limited by the modulation rate of the pattern projection and the sampling number (i.e., the number of patterns to recover an image). The modulation rate depends on a circuit's running speed and the rise and fall times of light emitters. The state of the art in the

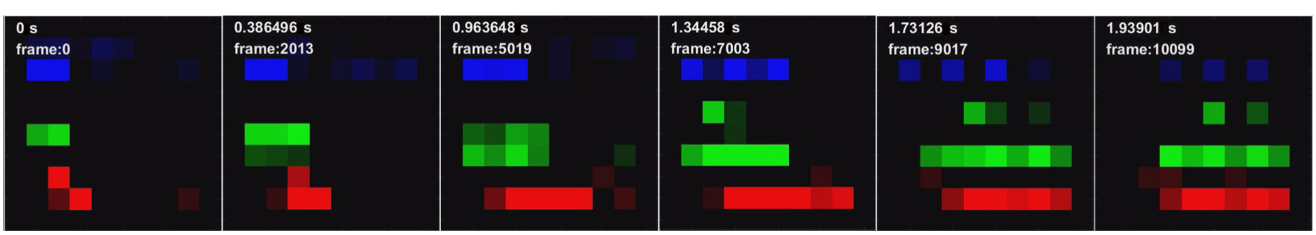

FIG. 4. Video screenshots from the color-imaging process. When the imager is capturing images, the object moves from left to right.

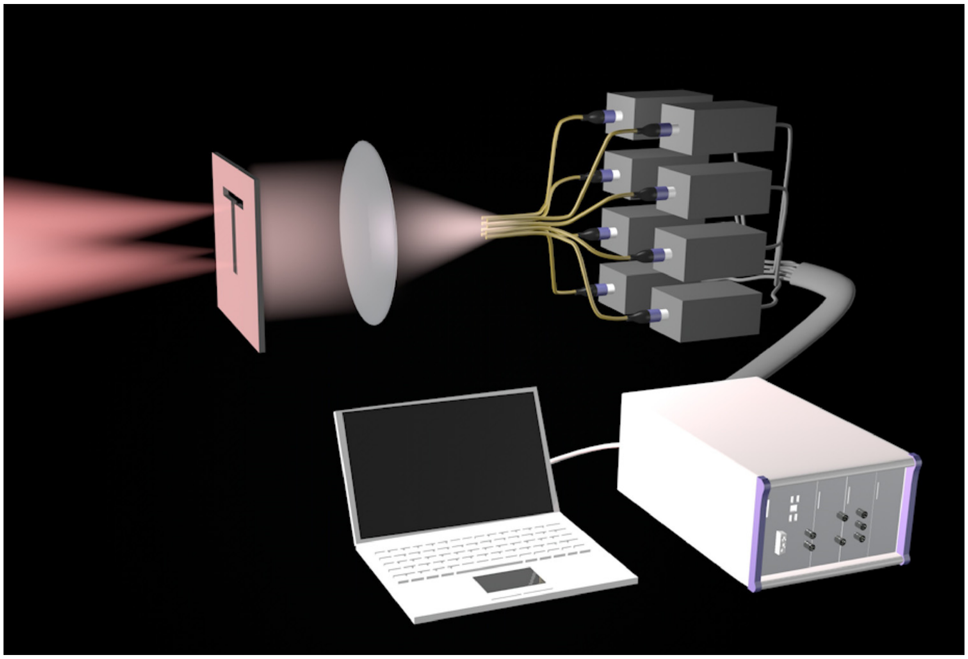

FIG. 5. Experimental scheme for low light-level imaging. The transmitted light from the object is collected by eight multimode fibers via a lens. Each fiber is connected to a SPD to count the number of photons reaching the detection plane.

semiconductor industry can provide a full-range modulation rate of more than 1 GHz. Many light sources, such as laser diodes, can have a rise or fall time of around a few tens of picoseconds. Thus, it will not be difficult to build a light-emitting array with a modulation rate of more than 1 GHz. In contrast, the sampling number largely affects the imaging speed. As the required spatial resolution of imaging increases, the sampling number increases accordingly, which slows down the imaging speed. However, with some algorithms such as compressive sensing [33–35] or deep learning [36–40], the sampling rate can be far below the Nyquist limit, which would dramatically increase the imaging frame rate, especially with prior knowledge of an object.

On the other hand, the high modulation rate is also subject both to the photosensitivity and the responsive bandwidth of a detector, especially in low light scenarios. To detect very weak light in a short time, one of the best types of detectors is the SPD array with a large number of pixels, which can provide a short overall dead time and a deep dynamic range. SPD arrays of 256 $\times$ 256 pixels were applied in a LIDAR system and excellent results were obtained [32]. We believe with a proper SPD array, a light-emission array, and a suitable algorithm, the proposed

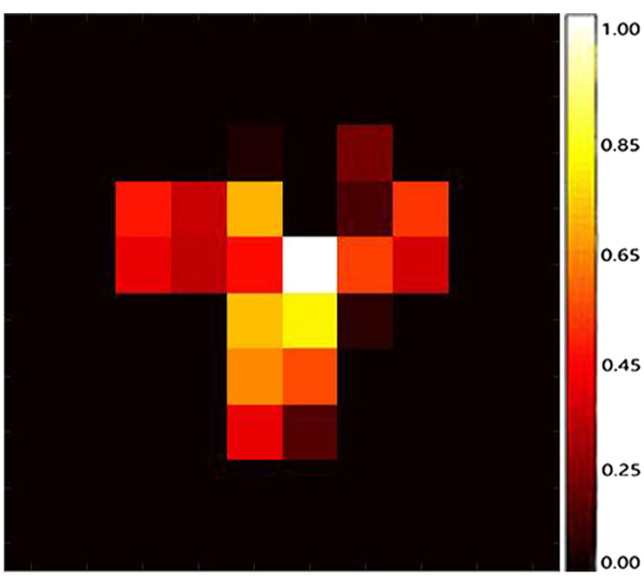

FIG. 6. Image of a letter T recovered in 700 μs. Eight single-photon detectors are used to collect the low photon flow wit a modulation rate of 1 MHz.

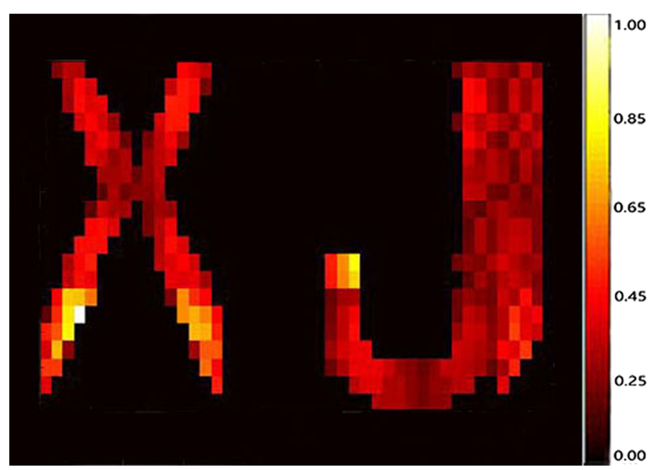

FIG. 7. Image of the object of characters XJ, which is reconstructed in 126 μs with 18 frames with a modulation rate of 10 MHz.

ghost-image scheme would become an excellent candidate method for a ultrahigh imaging frame rate under a low light level.

To realize colorful imaging, each element of the light-emitting array has three subpixels, which can display four states at each time: red, green, blue, and white (all *on*). If the circuit emits patterns in white, colorful imaging can be performed at a full-range modulation rate. To take most advantage of such fast emission, three bucket detectors are needed to measure the light intensities in red, green, and blue, respectively. If only one bucket detector is used, each pattern must be projected in red, green, and blue alternately, which reduces the imaging speed by a factor of 3 (as is done in the experiment). Moreover, the illuminating intensities and the detection sensitivities of the three colors should be prepared in specific ratios to guarantee the fidelity of the color reconstruction. When the above requirements are satisfied, a complete system is constructed for colorful imaging with a full modulation rate and a feasible fidelity of colors.

ACKNOWLEDGMENT

The work was supported by the National Natural Science Foundation of China (Grant No. 11503020).

[1] K. Goda, K. Tsia, and B. Jalali, Serial time-encoded amplified imaging for real-time observation of fast dynamic phenomena, Nature **458**, 1145 (2009).

[2] K. Nakagawa, A. Iwasaki, Y. Oishi, R. Horisaki, A. Tsukamoto, A. Nakamura, K. Hirosawa, H. Liao, T. Ushida, and K. A. Goda, Sequentially timed all-optical mapping photography (stamp), Nat. Photonics **8**, 695 (2014).

[3] T. Suzuki, F. Isa, L. Fujii, K. Hirosawa, K. Nakagawa, K. Goda, I. Sakuma, and F. Kannari, Sequentially timed all-optical mapping photography (stamp) utilizing spectral filtering, Opt. Express **23**, 30512 (2015).

[4] G. Gariepy, N. Krstajić, R. Henderson, C. Li, R. R. Thomson, G. S. Buller, B. Heshmat, R. Raskar, J. Leach, and D. Faccio, Single-photon sensitive light-in-fight imaging, Nat. Commun. **6**, 6021 (2015).

[5] P. Hockett and A. Stolow, Time-resolved imaging of purely valence-electron dynamics during a chemical reaction, Nat. Phys. **7**, 612 (2011).

[6] C. Y. Wong, R. M. Alvey, D. B. Turner, K. E. Wilk, D. A. Bryant, P. M. Curmi, R. J. Silbey, and G. D. Scholes, Electronic coherence lineshapes reveal hidden excitonic correlations in photosynthetic light harvesting, Nat. Chem. **4**, 396 (2012).

[7] Y. Acremann, C. H. Back, M. Buess, O. Portmann, A. Vaterlaus, D. Pescia, and H. Melchior, Imaging precessional motion of the magnetization vector, Science **290**, 492 (2000).

[8] T. Feurer, J. C. Vaughan, and K. A. Nelson, Spatiotemporal coherent control of lattice vibrational waves, Science **299**, 374 (2003).

[9] R. Kodama, P. A. Norreys, K. Mima, A. E. Dangor, R. G. Evans, H. Fujita, Y. Kitagawa, K. Krushelnick, T. Miyakoshi, and N. Miyanaga, Fast heating of ultrahigh-density plasma as a step towards laser fusion ignition, Nature **412**, 798 (2001).

[10] A. Velten, T. Willwacher, O. Gupta, A. Veeraraghavan, M. G. Bawendi, and R. Raskar, Recovering three-dimensional shape around a corner using ultrafast time-of-flight imaging, Nat. Commun. **3**, 745 (2012).

[11] J. Hajdu, R. Neutze, T. Sjögren, K. Edman, A. Szöke, R. C. Wilmouth, and C. M. Wilmot, Analyzing protein functions in four dimensions, Nat. Struct. Biol. **7**, 1006 (2000).

[12] A. H. Zewail, Four-dimensional electron microscopy, Science **328**, 187 (2010).

[13] A. Barty, S. Boutet, M. J. Bogan, S. Hau-Riege, S. Marchesini, K. Sokolowski-Tinten, N. Stojanovic, R. Tobey, H. Ehrke, and A. Cavalleri, Ultrafast single-shot diffraction imaging of nanoscale dynamics, Nat. Photonics **2**, 415 (2010).

[14] T. G. Etoh, A. Q. Nguyen, Y. Kamakura, K. Shimonomura, T. Y. Le, and N. Mori, The theoretical highest frame rate of silicon image sensors, Sensors **17**, 483 (2017).

[15] T. G. Etoh, C. Vo Le, Y. Hashishin, N. Otsuka, K. Takehara, H. Ohtake, T. Hayashida, and H. Maruyama, Evolution of ultra-high-speed ccd imagers, Plasma Fusion Res. **2**, S1021 (2007).

[16] L. Bian, J. Suo, G. Situ, Z. Li, J. Fan, F. Chen, and Q. Dai, Multispectral imaging using a single bucket detector, Sci. Rep. **6**, 24752 (2016).

[17] C. F. Higham, R. Murraysmith, M. J. Padgett, and M. P. Edgar, Deep learning for real-time single-pixel video, Sci. Rep. **8**, 2369 (2018).

[18] M. F. Duarte, M. A. Davenport, D. Takhar, J. N. Laska, T. Sun, K. F. Kelly, and R. G. Baraniuk, Single-pixel imaging via compressive sampling, IEEE Signal Process. Mag. **25**, 83 (2008).

[19] N. Radwell, K. J. Mitchell, G. M. Gibson, M. P. Edgar, R. Bowman, and M. J. Padgett, Single-pixel infrared and visible microscope, Optica **1**, 285 (2014).

[20] T. B. Pittman, Y. H. Shih, D. V. Strekalov, and A. V. Sergienko, Optical imaging by means of two-photon quantum entanglement, Phys. Rev. A. **52**, R3429 (1995).

[21] D. A. Zhang, Y. H. Zhai, L. A. Wu, and X. H. Chen, Correlated two-photon imaging with true thermal light, Opt. Lett. **30**, 2354 (2005).

[22] J. H. Shapiro, Computational ghost imaging, Phys, Rev. A **78**, 061802(R) (2008).

[23] Y. Bromberg, O. Katz, and Y. Silberberg, Ghost imaging with a single detector, Phys. Rev. A **79**, 053840 (2009).

[24] D. Pelliccia, A. Rack, M. Scheel, V. Cantelli, and D. M. Paganin, Experimental X-Ray Ghost Imaging, Phys. Rev. Lett. **117**, 113902 (2016).

[25] H. Yu, R. Lu, S. Han, H. Xie, G. Du, T. Xiao, and D. Zhu, Fourier-Transform Ghost Imaging with Hard X Rays, Phys. Rev. Lett. **117**, 113901 (2016).

[26] Z. Ai-Xin, H. Yu-Hang, W. Ling-An, C. Li-Ming, and W. Bing-Bing, Tabletop x-ray ghost imaging with ultra-low radiation, Optica **5**, 374 (2017).

[27] A. Schori and S. Shwartz, X-ray ghost imaging with a laboratory source, Opt. Express **25**, 14822 (2017).

[28] M. Lu, Ghost imaging via compressive sampling based on digital micromirror device, Acta Opt. Sin. **31**, 0711002 (2011).

[29] H. Chen, W. Zhao, H. Guo, B. Luo, J. Li, Y. Yuan, and Z. Xu, *A kind of ultrahigh speed real-time color calculates the device and method of ghost imaging*, China Patent No. CN107018388A (04 Aug. 2017).

[30] Z. H. Xu, W. Chen, J. Penuelas, M. Padgett, and M. J. Sun, 1000 fps computational ghost imaging using led-based structured illumination, Opt. Express **26**, 2427 (2018).

[31] J. A. Richardson, R. J. Walker, L. Grant, D. Stoppa, F. Borghetti, E. Charbon, M. Gersbach, and R. K. Henderson, in *IEEE Custom Integrated Circuits Conference* (San Jose, CA, 2009).

[32] L. Parmesan, N. Dutton, N. J. Calder, N. Krstajic, A. J. Holmes, L. A. Grant, and R. K. Henderson, in *International Image Sensor Workshop, Vaals, Netherlands, Memory* (Vaals, Netherlands, 2015), Vol. 900, p. M5.

[33] R. G. Baraniuk, Compressive sensing, IEEE Signal Process. Mag. **24** (2007).

[34] L. Xu, A. Sankaranarayanan, C. Studer, Y. Li, R. Baraniuk, and K. F. Kelly, in *Computational Optical Sensing and Imaging* (Optical Society of America, 2013), p. CW2C–4.

[35] T. Goldstein, L. Xu, K. F. Kelly, and R. Baraniuk, The stone transform: Multi-resolution image enhancement and compressive video, IEEE Trans. Image Process. **24**, 5581 (2015).

[36] L. Tao, C. Zhu, J. Song, T. Lu, H. Jia, and X. Xie, in *2017 IEEE International Conference on Image Processing (ICIP)* (IEEE, Beijing, 2017), p. 3215.

[37] L. Shen, Z. Yue, F. Feng, Q. Chen, S. Liu, and J. Ma, Msr-net: Low-light image enhancement using deep convolutional network, arXiv:1711.02488 (2017).

[38] L. Zhang, Z. Lin, R. He, Y. Qian, Q. Chen, and W. Zhang, Improving the noise immunity of 3d computational ghost imaging, Opt. Express **27**, 2344 (2019).

[39] Y. He, G. Wang, G. Dong, S. Zhu, H. Chen, A. Zhang, and Z. Xu, Ghost imaging based on deep learning, Sci. Rep. **8**, 6469 (2018).

[40] M. Lyu, W. Wang, H. Wang, H. Wang, G. Li, N. Chen, and G. Situ, Deep-learning-based ghost imaging, Sci. Rep. **7**, 17865 (2017).

[41] Please see the color.avi